
DiffEx: Explaining a Classifier with Diffusion Models to Identify Microscopic Cellular Variations

Anis Bourou^{*1,2} Saranga Kingkor Mahanta^{*1} Thomas Boyer¹ Valérie Mezger² Auguste Genovesio¹

Abstract

In recent years, deep learning models have been extensively applied to biological data across various modalities. Discriminative deep learning models have excelled at classifying images into categories (e.g., healthy versus diseased, treated versus untreated). However, these models are often perceived as black boxes due to their complexity and lack of interpretability, limiting their application in real-world biological contexts. In biological research, explainability is essential: understanding classifier decisions and identifying subtle differences between conditions are critical for elucidating the effects of treatments, disease progression, and biological processes. To address this challenge, we propose DiffEx, a method for generating visually interpretable attributes to explain classifiers and identify microscopic cellular variations between different conditions. We demonstrate the effectiveness of DiffEx in explaining classifiers trained on natural and biological images. Furthermore, we use DiffEx to uncover phenotypic differences within microscopy datasets. By offering insights into cellular variations through classifier explanations, DiffEx has the potential to advance the understanding of diseases and aid drug discovery by identifying novel biomarkers.

gus, 2014), particularly in microscopy images (Xing et al., 2018; Meijering, 2020), which poses challenges for the interpretability of these models. Explaining the decision-making processes of discriminative models is an active area of research. Various strategies (Selvaraju et al., 2017; Chattopadhyay et al., 2018; Lang et al., 2021a; Jeanneret et al., 2024; 2023) have been proposed to clarify how deep learning models arrive at their outputs, aiming to make the decision processes more transparent and understandable.

In biological imaging, interpreting classifier decisions is essential for understanding extracted features and uncovering biological insights. For instance, when classifying healthy versus diseased tissues or treated versus untreated samples, it is crucial to determine which attributes influence predictions. Identifying these cellular variations—phenotypes—not only deepens our understanding of diseases but also clarifies treatment effects. Thus, pinpointing the attributes that drive classifier outcomes is fundamental. By uncovering them, we can reveal biologically meaningful phenotypes that offer deeper insights into complex phenomena (Bourou & Genovesio, 2023; et al., 2022; Bourou et al., 2024).

In this work, we introduce **DiffEx**, a method for uncovering the attributes leveraged by a classifier to make its decisions, and demonstrate its effectiveness on both natural and microscopy images. Our method first builds a latent space that incorporates the classifier’s attributes using diffusion models. We then identify interpretable directions in this latent space using a contrastive learning approach. The discovered directions are ranked by selecting those that most significantly change the classifier’s decision.

We summarize our contributions in this work as follows:

- We introduce DiffEx, a novel method leveraging diffusion models to identify interpretable attributes that explain the decisions of a classifier.
- We demonstrate the versatility of DiffEx by applying it to classifiers trained on both natural and biological image datasets.
- In biological datasets, we employ DiffEx to uncover subtle cellular variations between different conditions.

1. Introduction

Image classification is a fundamental task in deep learning that has achieved remarkable results (Li et al., 2020; He et al., 2016; Huang et al., 2017; Dosovitskiy et al., 2020; Liu et al., 2022). The success of classifiers is primarily due to their ability to extract patterns and features from images to distinguish between classes. However, these patterns can often be difficult to discern (Li et al., 2020; Zeiler & Fer-

^{*}Equal contribution ¹ENS ²Université Paris Cité. Correspondence to: Auguste Genovesio <auguste.genovesio@bio.ens.psl.eu>.

2. Related Work

2.1. Classifiers Explainability

Class Activation Maps (CAMs) (Selvaraju et al., 2017; Chatopadhyay et al., 2018) are a well-known technique for explaining classifier decisions, as they highlight the most influential regions in an image that affect the classifier’s output. However, these methods typically require access to the classifier’s architecture and all its layers, as they involve computing gradients of the outputs with respect to the inputs. Additionally, CAMs only indicate important regions in images without explicitly identifying the affected attributes, such as shape, color, or size. This can be limiting, particularly in microscopy images where subtle variations are of interest. Counterfactual visual explanations represent another family of methods aimed at explaining classifier decisions. These methods seek to identify minimal changes that would alter the classifier’s decision. Generative models have been widely used to generate such counterfactual explanations. Generative Adversarial Networks (GANs), for instance, have been employed for this purpose (Singla et al., 2020; Lang et al., 2021a; Goetschalckx et al., 2019). While some approaches generate counterfactual explanations all at once (Singla et al., 2020; Goetschalckx et al., 2019), the work in (Lang et al., 2021a) identifies a set of attributes that influence the classifier’s decision. However, GANs suffer from training instability due to the simultaneous optimization of two networks: the generator and the discriminator. Recently, diffusion models have demonstrated more stable training, superior generation quality, and greater diversity (Dhariwal & Nichol, 2021; Nichol & Dhariwal, 2021). They have also been adopted for generating visual counterfactual explanations (Augustin et al., 2022; Jeanneret et al., 2024; Sobieski & Biecek, 2024).

2.2. Diffusion Models

Generative models have recently achieved significant success in various tasks (Goodfellow et al., 2014; Song & Ermon, 2020; Dhariwal & Nichol, 2021; Kingma & Welling, 2014). Diffusion models (Ho et al., 2020; Song et al., 2022; Dhariwal & Nichol, 2021; Nichol & Dhariwal, 2021), a class of generative models, have been applied to different domain (Dhariwal & Nichol, 2021; Guo et al., 2023; Rombach et al., 2022a). These models consist of two processes: a known forward process that gradually adds noise to the input data, and a learned backward process that iteratively denoises the noised input. Numerous works have proposed improvements to diffusion models (Dhariwal & Nichol, 2021; Rombach et al., 2022a; Nichol & Dhariwal, 2021), enhancing their performance and making them the new state-of-the-art in generative modeling across different tasks. Recently, it has been shown that diffusion models can be used to learn meaningful representations of images

that facilitate image editing tasks (Preechakul et al., 2022; Kwon et al., 2023). In (Preechakul et al., 2022), the authors proposed adding an encoder network during the training of diffusion models to learn a semantic representation of the image space. This approach enables the model to capture high-level features that can be manipulated for various applications. In (Kwon et al., 2023), the authors modified the reverse process—introducing an asymmetric reverse process—to discover semantic latent directions in the space induced by the bottleneck of the U-Net (Ronneberger et al., 2015) used as a denoiser in the diffusion model, which they refer to as the *h-space*. By exploring this space, they were able to identify directions corresponding to specific semantic attributes, allowing for targeted image modifications. These advancements demonstrate the potential of diffusion models not only for high-quality data generation but also for learning rich representations that can be leveraged for downstream tasks.

2.3. Detecting phenotypes in microscopy images

Capturing the visual cellular differences in microscopy images under varying conditions is essential for understanding certain diseases and the effects of treatments (Moshkov et al., 2022; Chandrasekaran et al., 2021; Lotfollahi et al., 2023; Bourou & Genovesio, 2023; et al., 2022; Bourou et al., 2024). Historically, hand-crafted methods were employed to measure changes between different conditions (et al., 2006). However, these tools have limitations, especially when the observed changes are subtle or masked by biological variability (et al., 2022; Bourou et al., 2024). Recently, generative models have been proposed to alleviate these limitations. In (Bourou & Genovesio, 2023), CycleGAN (Zhu et al., 2020) was used to perform image-to-image translations, aiming to discard biological variability and retain only the induced changes. By translating images from one condition to another, the model focused on the specific alterations caused by the experimental conditions, effectively highlighting phenotypic differences. In (et al., 2022), a conditional StyleGAN2 (Karras et al., 2020) was trained to identify phenotypes by interpolating between classes in the StyleGAN’s latent space. This approach enabled the generation of high-fidelity images that represent different phenotypic expressions, facilitating the study of subtle cellular variations and providing insights into the underlying biological processes. Furthermore, recent advancements have seen the use of conditional diffusion models in image-to-image translation (Bourou et al., 2024). In this method, an image from the source condition is first inverted into a latent code, that is used to generate corresponding the image from the target condition. This technique leverages the strengths of diffusion models in capturing complex data distributions and performing realistic translations between conditions. All of these methods have proven effective in

uncovering phenotypes and enhancing the understanding of cellular differences. However, they rely solely on generative models and do not integrate classifiers that can extract patterns from images and assess how a given image would be transferred to another class. Incorporating discriminative models alongside generative approaches could enhance pattern recognition and provide a more comprehensive analysis of cellular changes, ultimately improving the assessment of disease progression and treatment effects.

2.4. Contrastive learning

Contrastive learning is a powerful self-supervised framework that has achieved remarkable success across various domains, including computer vision and natural language processing (Chen et al., 2020; Radford et al., 2021; Gao et al., 2021; Fang et al., 2020). By contrasting positive and negative pairs, it learns rich feature representations, maximizing similarity for positive pairs while minimizing it for negative ones using a contrastive loss (Chen et al., 2020; van den Oord et al., 2019; Schroff et al., 2015; Wang & Liu, 2021). This versatile approach has been integrated into diverse architectures, enabling the extraction of robust and generalizable features for a wide range of downstream tasks. Beyond traditional applications, contrastive learning has also been leveraged in generative modeling. It has been employed to enhance conditioning in GANs (Kang & Park, 2020) and to improve style transfer in diffusion models (Yang et al., 2023). Discovering interpretable directions in generative models is fundamental to various image generation and editing tasks (Yüksel et al., 2021; Dalva & Yanardag, 2024; Kwon et al., 2023). In this context, contrastive learning has proven highly effective. For instance, LatentCLR (Yüksel et al., 2021) identifies meaningful transformations by applying contrastive learning to the latent space of GANs, while NoiseCLR (Dalva & Yanardag, 2024) uncovers semantic directions in pre-trained text-to-image diffusion models like Stable Diffusion (Rombach et al., 2022b).

3. Method

In this section, we introduce DiffEx, a method designed to explain a classifier by generating separable and interpretable attributes. As illustrated in Fig 1, our method leverages diffusion models to provide insights into the classifier’s behavior. First, we construct a latent semantic space that is aware of the classifier specific attributes. Then, using a contrastive learning approach, we identify separable and interpretable directions within this space. Finally, we rank the importance of the discovered directions and modify the image accordingly to highlight the critical features influencing the classifier’s predictions.

3.1. Building a classifier-aware semantic latent space

GANs benefit from a well-structured semantic latent space, which allows for easy control over different attributes of generated samples (Karras et al., 2019; 2020; Brock et al., 2019; Voynov & Babenko, 2020). This property has been leveraged in various applications, such as counterfactual visual explanations (Lang et al., 2021b). However, due to the iterative nature of diffusion models, they lack such a readily accessible latent space. In this work, we follow an approach similar to (Preechakul et al., 2022), where we construct a semantic latent space for our diffusion model by incorporating an encoder network. The encoder generates a latent code from a given input image, which is subsequently used to condition the diffusion process. To ensure that the generated samples maintain classifier-relevant attributes, we concatenate the classification score with the latent vector, forming a semantic code to condition the diffusion model, we denote it as z_{sem} .

$$L_{diffusion} = \sum_{t=1}^T \mathbb{E}_{x_0, \epsilon_t} \left[\|\epsilon_\theta(x_t, t, z_{sem}) - \epsilon_t\|_2^2 \right] \quad (1)$$

Indeed, our goal is not only to generate images using this semantic code, but also to ensure that the generated image retains the same classification score as the original input. To achieve this, we introduce a classifier loss, which in our case is a KL divergence between the classification scores of the input image x and the reconstructed one x' , an approach similar to (Lang et al., 2021b), the classifier loss is given by:

$$\mathcal{L}_{cls} = D_{KL} [C(x') || C(x)] \quad (2)$$

The total loss to optimize is then:

$$\mathcal{L}_{sem} = L_{diffusion} + \lambda_1 \mathcal{L}_{cls} \quad (3)$$

where λ_1 is a hyperparameter.

3.2. Finding interpretable directions in the latent space

After training our semantic encoder, we introduce a contrastive learning approach to identify distinct and interpretable directions within its latent space. Contrastive learning has shown strong potential in exploring the latent spaces of GANs (Yüksel et al., 2021) and has been adapted recently to discover latent directions in the noise space of text-to-image diffusion models (Dalva & Yanardag, 2024). Unlike these prior methods, which locate semantic directions within either an intermediate GAN layer or the noise space of a diffusion model, our approach focuses on identifying meaningful directions directly within the latent space of the learned encoder.

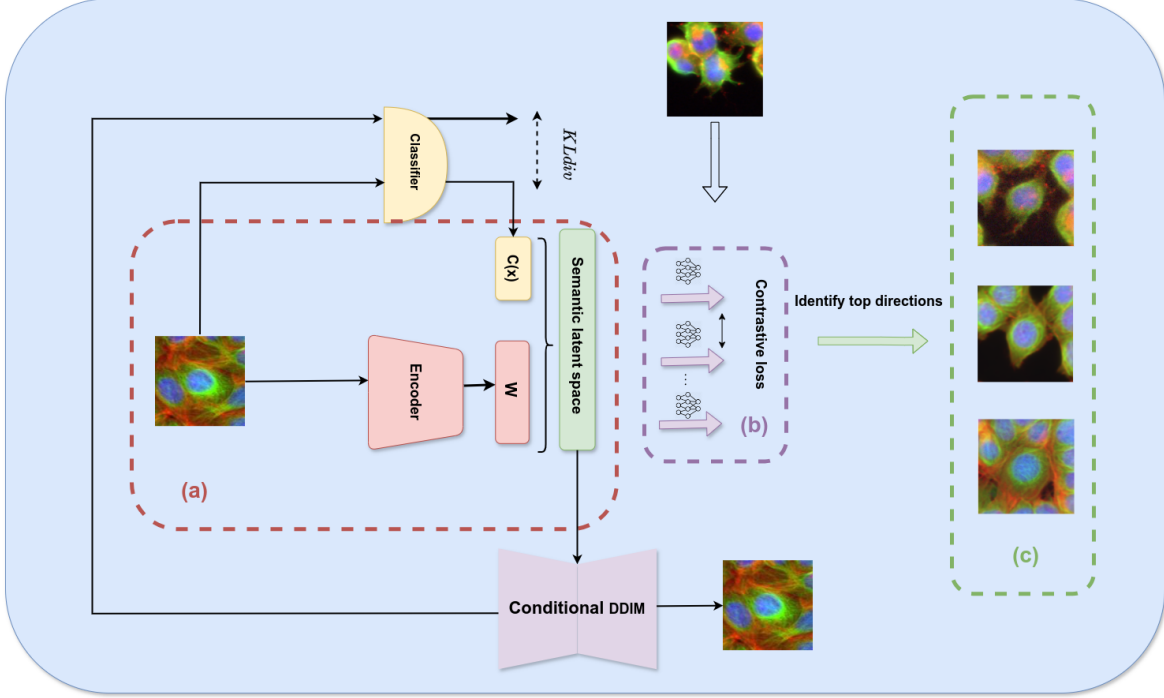


Figure 1. DiffEx primarily consists of three stages: **(a)** A semantic latent space is constructed by combining the embedding obtained from an encoder with the classifier’s prediction for each image. The resulting representation is used to condition the DDIM. **(b)** Directional models are learned in this semantic latent space using a self-supervised approach. **(c)** After identifying the directions that most significantly affect the classification probability, we shift the images accordingly. For example, in the accompanying figure, a single image is shifted along the identified directions, resulting in visibly different images that highlight the changes induced by these directions.

Formally, given an inverted image noise $x_T \in \mathcal{Z}_1$ and a semantic latent code $z_{sem} \in \mathcal{Z}_2$, we denote the diffusion models $\mathcal{DDIM} : \mathcal{Z}_1 \times \mathcal{Z}_2 \rightarrow \mathcal{X}$, where \mathcal{X} is the space of images. We aim to find directions $\Delta \mathbf{z}_1, \dots, \Delta \mathbf{z}_N$, $N > 1$ such that for $k < N$, $\mathcal{DDIM}(x_T, z_{sem} + \Delta \mathbf{z}_k)$ has visually meaningful changes compared to $\mathcal{DDIM}(x_T, z_{sem})$ while being similar to it.

Specifically, we want to learn a mapping $\mathcal{D}_k : \mathcal{Z}_2 \times \mathbb{R} \rightarrow \mathcal{Z}_2$ that takes as input a latent code z_{sem} and shift it along $\Delta \mathbf{z}_k$ with a weight α , ie, $\mathcal{D}_k : (z, \alpha) \rightarrow z + \Delta \mathbf{z}_k$. Similar to (Yüksel et al., 2021), we use multi-layer perceptron networks to learn the direction model \mathcal{D}_k as follows:

$$\mathcal{D}_k(z, \alpha) = z + \alpha \frac{\mathcal{MLP}_1(z)}{\|\mathcal{MLP}_1(z)\|} \quad (4)$$

For each latent code z_i , we shift it according to the N_{th} directional models, as follows:

$$\mathbf{z}_i^k = \mathcal{D}(z_i, \alpha) \quad (5)$$

Then, we pass it through another MLP to obtain intermediate feature representations,

$$\mathbf{h}_i^k = \mathcal{MLP}_2(z_i, \alpha) \quad (6)$$

After that, we compute the feature differences between the shifted and the original latent codes.

$$\mathbf{f}_i^k = \mathbf{h}_i^k - \mathcal{MLP}_2(z_i) \quad (7)$$

Following contrastive learning principles, we aim to increase the similarity between edits originating from the same directional model, encouraging them to attract each other. Conversely, we want edits from different directional models to repel each other by reducing their similarity. This objective can be expressed by the following contrastive equation:

$$\ell_{cont}(z_i^k) = -\log \frac{\sum_{j=1}^N \mathbf{1}_{[j \neq i]} \exp(\text{sim}(f_i^k, f_j^k)/\tau)}{\sum_{j=1}^N \sum_{l=1}^K \mathbf{1}_{[l \neq k]} \exp(\text{sim}(f_i^k, f_j^l)/\tau)} \quad (8)$$

The feature divergences obtained from the same directional model, represented as $\mathbf{f}_1^k, \mathbf{f}_2^k, \dots, \mathbf{f}_N^k$, are treated as *positive pairs*. We aim to maximize their similarity, contributing

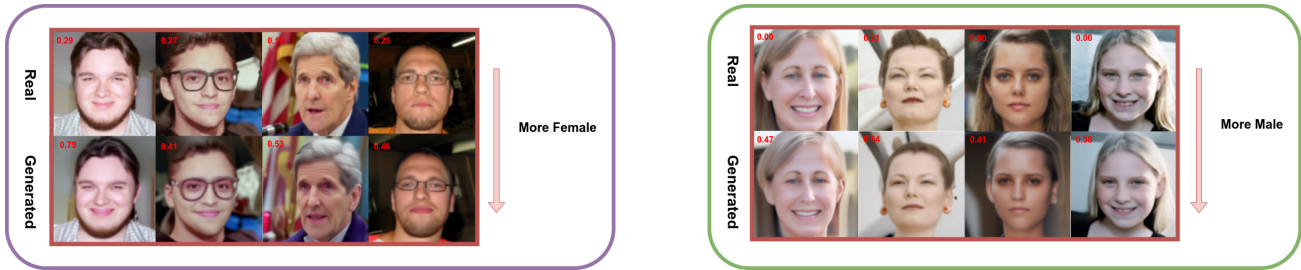
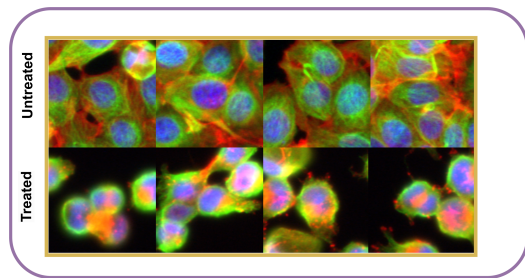
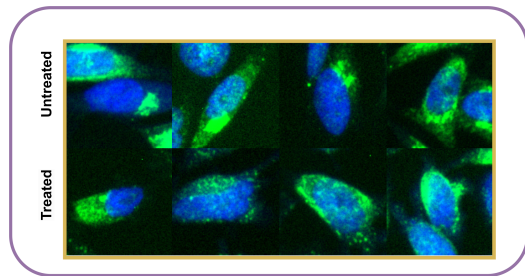


Figure 2. Shifting images toward the opposite class using directions identified by Diffex. **Left:** When transforming male images toward the female class, the appearance of lipstick becomes noticeable, suggesting it as a discriminative attribute for the classifier. **Right:** When shifting female images toward the male class, hairstyles tend to become shorter, indicating an attribute associated with the male class. The probabilities of the target classes are shown in red.



(a)



(b)

Figure 3. Images from two datasets: (a) BBBC021 dataset and (b) Golgi dataset. While the differences between the two classes are apparent in BBBC021—such as the disappearance of the cytoplasm and fewer nuclei—they are more subtle in the Golgi dataset.

to the numerator of the loss function. Conversely, feature divergences originating from different directional models (e.g., $\mathbf{f}_1^k \neq \mathbf{f}_1^l, l \neq k$) are treated as *negative pairs*. For these, we seek to minimize similarity, thus they contribute to the denominator of the loss function.

On top of the contrastive loss, we introduce a regularization term that promotes further decorrelation between the learned directions by minimizing the off-diagonal elements of the covariance matrix associated with the different directional models. This approach is inspired by (Bardes et al., 2022),

and the regularization term is defined as follows:

$$\mathcal{L}_{\text{reg}} = \sum_{i \neq j} \text{Cov}(\mathcal{D}_i(z), \mathcal{D}_j(z))^2 \quad (9)$$

Finally, we minimize this following total loss to learn the direction models:

$$\mathcal{L}_{\text{dir}} = L_{\text{cont}} + \lambda_2 \mathcal{L}_{\text{reg}} \quad (10)$$

where λ_1 is a hyperparameter.

3.3. Ranking the identified direction according to their importance

After obtaining the directional models, the next step is to identify those that significantly influence the classifier’s probabilities. To do this, we first select a sample of images and compute their initial classification scores. For each discovered direction, we shift all images in the sample along that direction by a specific value of α and then calculate the new classification scores for the shifted images. If the average change in classification scores exceeds a predefined threshold, we retain that direction. Once a direction is selected, the images used to explain it are removed from the sample to avoid redundancy. This process is repeated iteratively until we identify the desired number of directions or exhaust the available images. The detailed pseudo-code for this procedure is provided in the Supplementary. B.

4. Results

4.1. Datasets

We used the following datasets to evaluate our method:

FFHQ: The FFHQ (Karras et al., 2019) dataset is a high-quality image collection containing 70,000 high-resolution face images with diverse variations. Given its combination of high resolution and diversity, FFHQ has become a benchmark in the field.

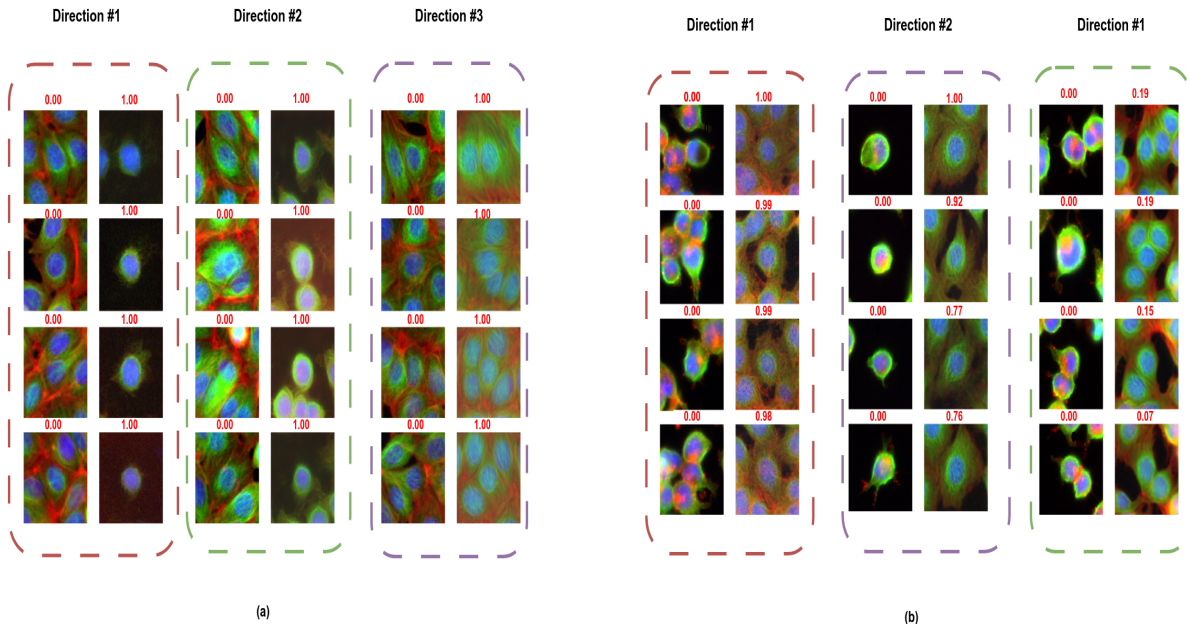


Figure 4. Shifting images toward the opposite class. **Left:** DiffEx identified three distinct directions for transitioning from the untreated to the treated class. Direction 1 eliminates the cytoplasm and most cells, leaving a single nucleus at the center. Direction 2 removes the cytoplasm without eliminating all nuclei. Direction 3 tends to cluster nuclei closer together and decreases the intensity of the red channel. **Right:** To shift from the treated to the untreated class, Direction 1 increases the intensity of the red channel and pushes nuclei apart. Direction 2 enhances the green channel, while Direction 3 increases the cell count, replicating known phenotypes

BBBC021: The BBBC021 dataset (et al., 2010) is a publicly available collection of fluorescent microscopy images of MCF-7, a breast cancer cell line treated with 113 small molecules at eight different concentrations. For our research, we focused on images of untreated cells and cells treated with the highest concentration of the compound Latrunculin B. In Fig. 3, the green, blue, and red channels label for B-tubulin, DNA, and F-actin respectively.

Golgi: Fluorescent microscopy images of HeLa cells untreated (DMSO) and treated with Nocodazole. In Fig. 3, the green and blue channels label for B-tubulin and DNA respectively.

4.2. DiffEx encodes natural and biological images

We trained a classifier on the FFHQ dataset to distinguish between male and female classes, we also trained classifiers on BBBC021 and Golgi datasets to classify untreated and treated images. As shown in Table 1, the proposed framework effectively encodes both biological and natural image features. Indeed, the different metrics used to assess the reconstruction quality demonstrate very low values for the datasets utilized in the experiments. Furthermore, the classification metrics across the three classifiers perform well on the generated images. This consistent classification accuracy suggests that the generated images are not only vi-

sually coherent but also maintain key distinguishing features necessary for correct classification, most importantly, the absence of adversarial artifacts that could alter the classifier’s decisions.

Table 1. Comparison of metrics for different datasets, including classification accuracy.

Dataset	LPIPS	SSIM	MSE	Accuracy
BBBC021	0.0237	0.99	0.0007	100
FFHQ/gender	0.0118	1.0	0.0004	99.5
Golgi	0.0594	1.0	0.0003	95

4.3. Explaining a Classifier trained on natural and biological images

First, we applied DiffEx to explain a classifier trained on natural images. In Fig. 2, some directions identified by the method on the FFHQ dataset are shown. Specifically, short haircuts tend to push the classification toward the “male” class, while the presence of lipstick pushes the classification toward the “female” class, more examples are shown in Supplementary. A

We then applied DiffEx to a classifier trained on the BBBC021 images. In Fig.4, we illustrate the three most significant directions identified by our method for transition-

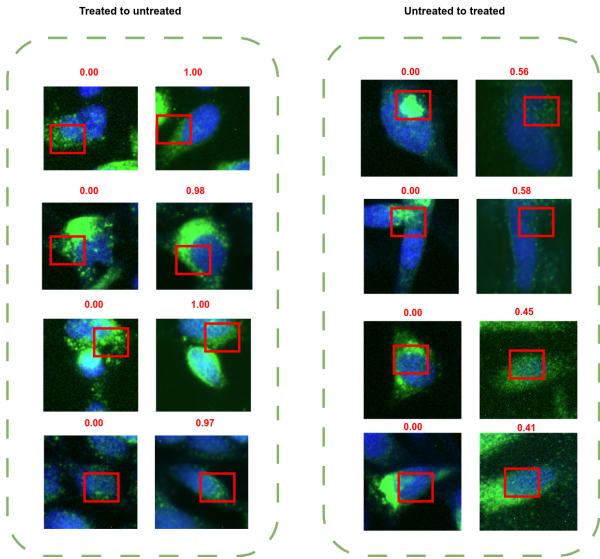


Figure 5. Shifting images toward the opposite class. **Left:** When transitioning from the treated to the untreated class, the Golgi apparatus tends to aggregate. **Right:** Conversely, shifting from the untreated to the treated class results in its dispersion. These observations replicate the phenotypic effects of the treatment, which induces Golgi apparatus scattering.

ing between the treated and untreated cases. Each direction leads to distinct outputs, demonstrating that the directions are well disentangled and separated. These directions replicate various phenotypic aspects induced by the treatment administered to the cells. As shown in Fig.3, the drug’s toxicity causes cell death, leading to the disappearance of cytoplasm and a reduction in nuclei count. Direction 1 replicates this phenotype: the generated image displays only a single nucleus centered in the frame, with the cytoplasm entirely absent. In contrast, Direction 2 does not entirely eliminate the cells but removes most of the cytoplasm, a hallmark of the treatment effect. Direction 3 maintains the cell count and partially retains the cytoplasm but reduces the intensity of the red channel, it also tends to cluster the nuclei closer together.

For the reverse case shown in Fig. 4, directions were identified for transitioning from the treated to the untreated class. Direction 1 adds cytoplasm back and increases the distance between nuclei, effectively reversing the phenotype of Direction 3 from the untreated-to-treated transition. Direction 2 restores cytoplasm while keeping the nuclei count constant. Finally, Direction 3 increases the number of nuclei and slightly restores cytoplasm between them.

Lastly, we tested our method on another dataset, the Golgi dataset. These images depict cells treated with Nocodazole, which causes the Golgi apparatus to scatter. This phenotype can be subtle and challenging to observe. Using CellProfiler,

we confirmed this phenotype by measuring the area occupied by the Golgi apparatus in both untreated and treated cases. As shown in Fig., the Golgi apparatus occupies a larger area in the untreated case due to its scattering.

In Fig. 5, we highlight the most significant direction identified by the method. For the untreated-to-treated transition, the Golgi apparatus becomes more scattered, replicating the effect of the treatment. Conversely, for the treated-to-untreated transition, the Golgi apparatus becomes more aggregated, effectively mimicking the reversal of the treatment’s effect. In contrast to the BBBC021 dataset, all the identified directions replicate exactly the same phenotypes. This could be due to the limited number of channels used in this dataset (green and blue only).

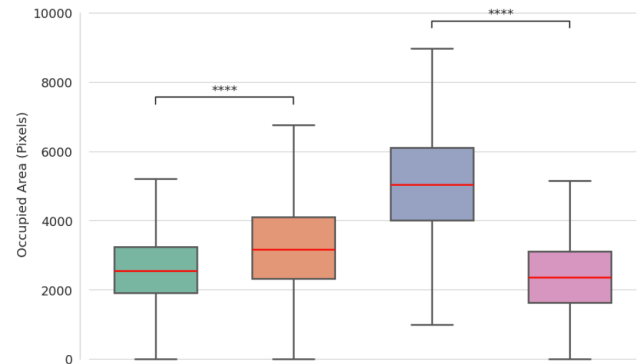


Figure 6. **Left:** Measurement of the Golgi apparatus area in real images for both conditions reveals a difference in its spatial distribution. The area is larger in the treated case due to treatment-induced scattering. **Right:** Measurement of the nuclear area in the BBBC021 dataset shows that it is larger in the untreated case. This is attributed to the treatment’s toxicity, which eliminates cells, reducing overall nuclear presence

4.4. Comparing to existing methods

Comparing our method to existing approaches is inherently challenging, as many of the current methods for detecting phenotypes rely solely on generative models. Among the most closely related methods, *GCD*(Sobieski & Biecek, 2024) stands out, although it was not proposed to identify phenotypes, it uses diffusion models to explain a classifier. Similar to our approach, they utilize a latent space constructed with DiffAE(Preechakul et al., 2022). However, *GCD* does not incorporate the classifier during training, and it identifies counterfactual directions using a single image optimized to minimize a counterfactual loss.

For comparison, we identified the first principal direction that most significantly shifts the classification score of the trained classifier. In Fig. 7, we present the generated explanation using our method and *GCD*. It is evident that the explanations produced by our method are visually superior

Table 2. Performance metrics of our method compared to GCD. A '-' indicates that no explanation was found

Method	Gender		BBBC021		Golgi	
	KID	SSIM	KID	SSIM	KID	SSIM
GCD	0.13	0.55	-	-	-	-
Ours	0.12	0.67	0.07	0.22	0.032	0.69

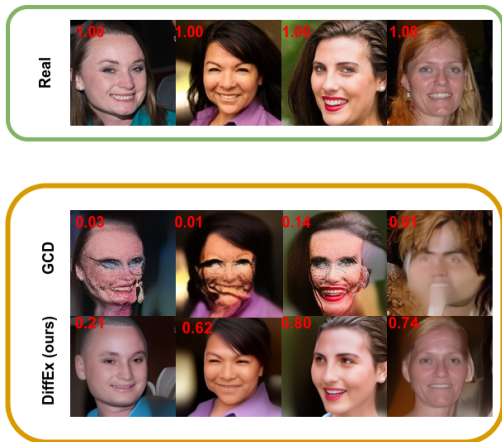


Figure 7. Generating counterfactual explanation with our method and GCD. We can see that our method gives visually better and more disentangled results.

and more disentangled compared to those obtained using GCD. Specifically, our method focus on modifying a single attribute—primarily shortening the hairstyle—while GCD introduces changes to multiple attributes simultaneously, leading to less interpretable results. Additionally, we observe that the classification shifts are more pronounced in the examples generated by GCD compared to those produced by our method. This can be attributed to GCD’s optimization of the counterfactual loss with respect to shifts in latent space. While GCD can identify a direction that reduces the classifier’s confidence, the resulting counterfactuals are often of poor visual quality, as evident in some of the generated samples. In Fig. 4, we further evaluate the performance of GCD and our method on biological images. Notably, GCD fails to generate meaningful images when applied to this domain. This limitation is likely due to GCD’s reliance on a single image to identify directions in the learned latent space. While this approach works well in datasets with inherent class similarities, such as FFHQ, it struggles in scenarios where there is high variability between classes, as is the case with biological images. Furthermore, in Table 2, we compare the quality of the generated explanations using the Kernel Inception Distance (KID) (Bińkowski et al., 2021), as well as the similarity between the original and generated images. The results show that our method consistently outperforms GCD across various datasets. This indicates that our method produces images that are not only closer to the

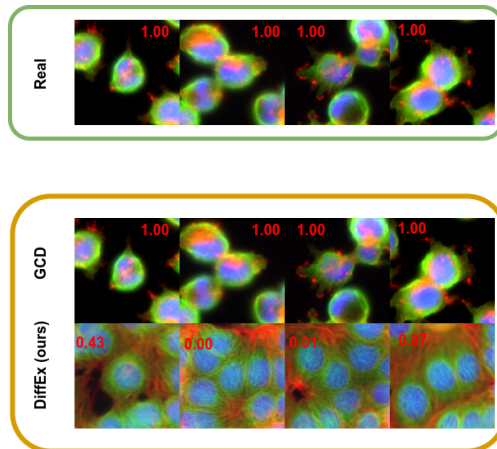


Figure 8. Generating counterfactual explanations with our method and GCD reveals that GCD fails to generate counterfactuals for biological datasets. This limitation may be due to its reliance on a single image to identify directions in the latent space, which proves challenging for datasets with high variability, such as biological data.

target dataset distribution but also retain higher similarity to the original images, demonstrating its effectiveness and robustness.

5. Conclusion

In this work, we introduced DiffEx, a versatile framework for explaining classifiers using diffusion models. By identifying meaningful directions in the latent space, DiffEx produces high-quality and disentangled attributes that maintain fidelity to the original data while effectively shifting classification outcomes. An important application of DiffEx is its ability to detect phenotypes. We validated this capability across multiple datasets, demonstrating that DiffEx can reveal fine-grained biological variations and enhance our understanding of cellular and phenotypic differences. This highlights the method’s potential to be a valuable tool in advancing research in biology and related fields, where uncovering subtle variations is essential. Moreover, DiffEx can be extended to other applications where it is critical to explain classifier outputs, making it a versatile framework for enhancing model interpretability across diverse domains.

References

- Augustin, M., Boreiko, V., Croce, F., and Hein, M. Diffusion visual counterfactual explanations. In *Advances in Neural Information Processing Systems (NeurIPS)*, 2022.
- Bardes, A., Ponce, J., and LeCun, Y. VICReg: Variance-invariance-covariance regularization for self-supervised learning. In *International Conference on Learning Representations*, 2022. URL <https://openreview.net/forum?id=xm6YD62D1Ub>.
- Bińkowski, M., Sutherland, D. J., Arbel, M., and Gretton, A. Demystifying mmd gans, 2021. URL <https://arxiv.org/abs/1801.01401>.
- Bourou, A. and Genovesio, A. Unpaired image-to-image translation with limited data to reveal subtle phenotypes, 2023.
- Bourou, A., Boyer, T., Gheisari, M., Daupin, K., Dubreuil, V., De Thonel, A., Mezger, V., and Genovesio, A. Phen-Diff: Revealing Subtle Phenotypes with Diffusion Models in Real Images . In *proceedings of Medical Image Computing and Computer Assisted Intervention – MICCAI 2024*, volume LNCS 15003. Springer Nature Switzerland, October 2024.
- Brock, A., Donahue, J., and Simonyan, K. Large scale GAN training for high fidelity natural image synthesis. In *International Conference on Learning Representations (ICLR)*, 2019. URL <https://openreview.net/forum?id=B1xsqj09Fm>.
- Chandrasekaran, S. N. C., Ceulemans, H., Boyd, J. D., and Carpenter, A. E. Image-based profiling for drug discovery: due for a machine-learning upgrade? *Nature Reviews Drug Discovery*, 20:145–159, 2021. doi: 10.1038/s41573-020-00117-w.
- Chattopadhyay, A., Sarkar, A., Howlader, P., and Balasubramanian, V. N. Grad-cam++: Improved visual explanations for deep convolutional networks. In *2018 IEEE Winter Conference on Applications of Computer Vision (WACV)*, pp. 839–847. IEEE, 2018.
- Chen, T., Kornblith, S., Norouzi, M., and Hinton, G. A simple framework for contrastive learning of visual representations. In *International Conference on Machine Learning*, pp. 1597–1607, 2020.
- Dalva, Y. and Yanardag, P. Noiseclr: A contrastive learning approach for unsupervised discovery of interpretable directions in diffusion models. In *Proceedings of the IEEE/CVF Conference on Computer Vision and Pattern Recognition (CVPR)*, pp. 24209–24218, June 2024.
- Dhariwal, P. and Nichol, A. Diffusion models beat gans on image synthesis, 2021.
- Dosovitskiy, A., Beyer, L., Kolesnikov, A., Weissenborn, D., Zhai, X., Unterthiner, T., Dehghani, M., Minderer, M., Heigold, G., Gelly, S., Uszkoreit, J., and Houslsby, N. An image is worth 16x16 words: Transformers for image recognition at scale. *arXiv preprint arXiv:2010.11929*, 2020.
- et al, A. C. Cellprofiler: Image analysis software for identifying and quantifying cell phenotypes. *Genome biology*, 7:R100, 02 2006. doi: 10.1186/gb-2006-7-10-r100.
- et al., A. L. Revealing invisible cell phenotypes with conditional generative modeling. *Nature Communications*, 14, 2022. URL <https://api.semanticscholar.org/CorpusID:249873188>.
- et al., P. D. C. High-Content Phenotypic Profiling of Drug Response Signatures across Distinct Cancer Cells. *Molecular Cancer Therapeutics*, 9(6):1913–1926, 06 2010. ISSN 1535-7163. doi: 10.1158/1535-7163.MCT-09-1148. URL <https://doi.org/10.1158/1535-7163.MCT-09-1148>.
- Fang, M., Smith, A., Guo, H., et al. Cert: Contrastive self-supervised learning for language understanding. *arXiv preprint arXiv:2005.12766*, 2020.
- Gao, T., Yao, X., and Chen, D. Simcse: Simple contrastive learning of sentence embeddings. In *Proceedings of the 2021 Conference on Empirical Methods in Natural Language Processing*, pp. 6894–6910, 2021.
- Goetschalckx, L., Andonian, A., Oliva, A., and Isola, P. Ganalyze: Toward visual definitions of cognitive image properties. In *Proceedings of the IEEE/CVF International Conference on Computer Vision (ICCV)*, pp. 5743–5752, October 2019. doi: 10.1109/ICCV.2019.00584.
- Goodfellow, I. J., Pouget-Abadie, J., Mirza, M., Xu, B., Warde-Farley, D., Ozair, S., Courville, A., and Bengio, Y. Generative adversarial networks, 2014.
- Guo, Z., Liu, J., Wang, Y., Chen, M., Wang, D., Xu, D., and Cheng, J. Diffusion models in bioinformatics: A new wave of deep learning revolution in action. *CoRR*, abs/2302.10907, 2023. URL <https://arxiv.org/abs/2302.10907>.
- He, K., Zhang, X., Ren, S., and Sun, J. Deep residual learning for image recognition. In *Proceedings of the IEEE conference on computer vision and pattern recognition (CVPR)*, pp. 770–778, 2016.
- Ho, J., Jain, A., and Abbeel, P. Denoising diffusion probabilistic models, 2020.
- Huang, G., Liu, Z., Van Der Maaten, L., and Weinberger, K. Q. Densely connected convolutional networks. In

-
- Proceedings of the IEEE conference on computer vision and pattern recognition (CVPR)*, pp. 4700–4708, 2017.
- Jeanneret, G., Simon, L., and Jurie, F. Adversarial counterfactual visual explanations. In *Proceedings of the IEEE/CVF Conference on Computer Vision and Pattern Recognition (CVPR)*, pp. 16425–16435, June 2023.
- Jeanneret, G., Simon, L., and Jurie, F. Text-to-image models for counterfactual explanations: A black-box approach. In *Proceedings of the IEEE/CVF Winter Conference on Applications of Computer Vision (WACV)*, pp. 4757–4767, January 2024.
- Kang, M. and Park, J. Contragan: Contrastive learning for conditional image generation. In *Advances in Neural Information Processing Systems*, volume 33, pp. 21312–21323, 2020.
- Karras, T., Laine, S., and Aila, T. A style-based generator architecture for generative adversarial networks. In *Proceedings of the IEEE/CVF Conference on Computer Vision and Pattern Recognition (CVPR)*, pp. 4401–4410, 2019.
- Karras, T., Laine, S., Aittala, M., Hellsten, J., Lehtinen, J., and Aila, T. Analyzing and improving the image quality of StyleGAN. In *Proc. CVPR*, 2020.
- Kingma, D. P. and Welling, M. Auto-encoding variational bayes. *Proceedings of the International Conference on Learning Representations (ICLR)*, 2014. URL <https://arxiv.org/abs/1312.6114>.
- Kwon, M., Jeong, J., and Uh, Y. Diffusion models already have a semantic latent space, 2023. URL <https://arxiv.org/abs/2210.10960>.
- Lang, O., Gandelsman, Y., Yarom, M., Wald, Y., Elidan, G., Hassidim, A., Freeman, W. T., Isola, P., Globerson, A., Irani, M., and Mosseri, I. Explaining in style: Training a gan to explain a classifier in stylespace. In *Proceedings of the IEEE/CVF International Conference on Computer Vision (ICCV)*, October 2021a.
- Lang, O., Gandelsman, Y., Yarom, M., Wald, Y., Elidan, G., Hassidim, A., Freeman, W. T., Isola, P., Globerson, A., Irani, M., and Mosseri, I. Explaining in style: Training a gan to explain a classifier in stylespace. *arXiv preprint arXiv:2104.13369*, 2021b.
- Li, Z., Yang, W., Peng, S., and Liu, F. A survey of convolutional neural networks: Analysis, applications, and prospects, 2020.
- Liu, Z., Mao, H., Wu, C.-Y., Feichtenhofer, C., Darrell, T., and Xie, S. A convnet for the 2020s. *arXiv preprint arXiv:2201.03545*, 2022.
- Lotfollahi, M., Klimovskaia Susmelj, A., De Donno, C., Hetzel, L., Ji, Y., Ibarra, I. L., Srivatsan, S. R., Naghipourfar, M., Daza, R. M., Martin, B., Shendure, J., McFaline-Figueroa, J. L., Boyeau, P., Wolf, F. A., Yakubova, N., Günnemann, S., Trapnell, C., Lopez-Paz, D., and Theis, F. J. Predicting cellular responses to complex perturbations in high-throughput screens. *Molecular Systems Biology*, 19(6), 2023. doi: 10.15252/msb.202211517.
- Meijering, E. A bird’s-eye view of deep learning in bioimage analysis. *Computational and Structural Biotechnology Journal*, 18:2312–2325, 2020. ISSN 2001-0370. doi: <https://doi.org/10.1016/j.csbj.2020.08.003>. URL <https://www.sciencedirect.com/science/article/pii/S2001037020303561>.
- Moshkov, N., Bornholdt, M., Benoit, S., Smith, M., McQuin, C., Goodman, A., Senft, R., Han, Y., Babadi, M., Horvath, P., Cimini, B. A., Carpenter, A. E., Singh, S., and Caicedo, J. C. Learning representations for image-based profiling of perturbations. *bioRxiv*, 2022. doi: 10.1101/2022.08.12.503783. URL <https://www.biorxiv.org/content/early/2022/08/15/2022.08.12.503783>.
- Nichol, A. Q. and Dhariwal, P. Improved denoising diffusion probabilistic models. In Meila, M. and Zhang, T. (eds.), *Proceedings of the 38th International Conference on Machine Learning*, volume 139 of *Proceedings of Machine Learning Research*, pp. 8162–8171. PMLR, 18–24 Jul 2021. URL <https://proceedings.mlr.press/v139/nichol21a.html>.
- Preechakul, K., Chatthee, N., Wizadwongsa, S., and Suwajanakorn, S. Diffusion autoencoders: Toward a meaningful and decodable representation. In *Proceedings of the IEEE/CVF Conference on Computer Vision and Pattern Recognition (CVPR)*, pp. 10657–10667, 2022. doi: 10.1109/CVPR52688.2022.01039. URL <https://Diff-AE.github.io/>.
- Radford, A., Kim, J. W., Hallacy, C., Ramesh, A., Goh, G., Agarwal, S., Sastry, G., Askell, A., Mishkin, P., Clark, J., et al. Learning transferable visual models from natural language supervision. In *International Conference on Machine Learning*, 2021.
- Rombach, R., Blattmann, A., Lorenz, D., Esser, P., and Ommer, B. High-resolution image synthesis with latent diffusion models. In *Proceedings of the IEEE/CVF Conference on Computer Vision and Pattern Recognition (CVPR)*, pp. 10684–10695, 2022a. doi: 10.1109/CVPR52688.2022.01042.
- Rombach, R., Blattmann, A., Lorenz, D., Esser, P., and Ommer, B. High-resolution image synthesis with latent diffusion models. In *Proceedings of the IEEE/CVF*

-
- Conference on Computer Vision and Pattern Recognition (CVPR)*, pp. 10684–10695, June 2022b. doi: 10.1109/CVPR52688.2022.01045. URL <https://arxiv.org/abs/2112.10752>.
- Ronneberger, O., Fischer, P., and Brox, T. U-net: Convolutional networks for biomedical image segmentation. *CoRR*, abs/1505.04597, 2015. URL <http://arxiv.org/abs/1505.04597>.
- Schroff, F., Kalenichenko, D., and Philbin, J. Facenet: A unified embedding for face recognition and clustering. In *Proceedings of the IEEE conference on computer vision and pattern recognition*, pp. 815–823, 2015.
- Selvaraju, R. R., Cogswell, M., Das, A., Vedantam, R., Parikh, D., and Batra, D. Grad-cam: Visual explanations from deep networks via gradient-based localization. In *Proceedings of the IEEE International Conference on Computer Vision (ICCV)*, pp. 618–626, 2017.
- Singla, S., Pollack, B., Chen, J., and Batmanghelich, K. Explanation by progressive exaggeration. In *Proceedings of the International Conference on Learning Representations (ICLR)*, 2020. URL <https://openreview.net/forum?id=r1xDBaEKvH>.
- Sobieski, B. and Biecek, P. Global counterfactual directions. In *Proceedings of the European Conference on Computer Vision (ECCV)*, 2024. doi: 10.48550/ARXIV.2404.12488. URL <https://arxiv.org/abs/2404.12488>.
- Song, J., Meng, C., and Ermon, S. Denoising diffusion implicit models, 2022.
- Song, Y. and Ermon, S. Generative modeling by estimating gradients of the data distribution, 2020.
- van den Oord, A., Li, Y., and Vinyals, O. Representation learning with contrastive predictive coding, 2019. URL <https://arxiv.org/abs/1807.03748>.
- Voynov, A. and Babenko, A. Unsupervised discovery of interpretable directions in the GAN latent space. In *Proceedings of the 37th International Conference on Machine Learning (ICML)*, volume 119 of *Proceedings of Machine Learning Research*, pp. 9786–9796. PMLR, 2020. URL <https://proceedings.mlr.press/v119/voynov20a.html>.
- Wang, F. and Liu, H. Understanding the behaviour of contrastive loss. In *Proceedings of the IEEE/CVF Conference on Computer Vision and Pattern Recognition*, pp. 2495–2504, 2021.
- Xing, F., Xie, Y., Su, H., Liu, F., and Yang, L. Deep learning in microscopy image analysis: A survey. *IEEE Transactions on Neural Networks and Learning Systems*, 29(10): 4550–4568, 2018. doi: 10.1109/TNNLS.2017.2766168.
- Yang, S., Hwang, H., and Ye, J. C. Zero-shot contrastive loss for text-guided diffusion image style transfer. In *Proceedings of the IEEE/CVF International Conference on Computer Vision (ICCV)*, 2023. URL https://openaccess.thecvf.com/content/ICCV2023/html/Yang_Zero-Shot_Contrastive_Loss_for_Text-Guided_Diffusion_Image_Style_Transfer_ICCV_2023_paper.html.
- Yüksel, O. K., Simsar, E., Er, E. G., and Yanardag, P. Latentclr: A contrastive learning approach for unsupervised discovery of interpretable directions. In *Proceedings of the IEEE/CVF International Conference on Computer Vision (ICCV)*, pp. 14263–14272, October 2021.
- Zeiler, M. D. and Fergus, R. Visualizing and understanding convolutional networks. In Fleet, D., Pajdla, T., Schiele, B., and Tuytelaars, T. (eds.), *Computer Vision – ECCV 2014*, pp. 818–833, Cham, 2014. Springer International Publishing. ISBN 978-3-319-10590-1.
- Zhu, J.-Y., Park, T., Isola, P., and Efros, A. A. Unpaired image-to-image translation using cycle-consistent adversarial networks, 2020.

A. More examples

In the following examples, we trained DiffeEX to identify 10 different directions in the semantic space. As we can see, these directions alter various attributes, but not all of them lead to changes in the output probabilities. To address this, we apply our ranking algorithm to rank the directions based on their ability to modify the classification output. For instance, in this case, the most important attribute is direction 5 (positive), which shortens the haircut of images belonging to the female class. Conversely, direction 6 (negative) adds makeup to images of males, increasing the probability of classification into the female class.



B. Ranking Algorithm Pseudo-code

Algorithm 1 Ranking algorithm

Data: Model f , Diff-Ex Generator G , Number of samples $n_{samples}$, Number of directions n_{dirs} , Alpha α , Threshold τ , Max coordinates M

Result: Best coordinates C and directions D

Initialize empty lists $C \leftarrow []$, $D \leftarrow []$ Initialize used coordinates $U \leftarrow \emptyset$ Sample $n_{samples}$ images from the dataset pertaining to a particular class

while $length(C) < M$ **do**

- $max_effect \leftarrow 0$, $best_coordinate \leftarrow None$, $best_direction \leftarrow None$
- for** each image batch B of size BS from the remaining images **do**
 - Encode B to obtain the semantic space: $z_{sem} \leftarrow G.encode(B)$
 - Encode the stochastic latent code: $x_T \leftarrow G.encode_stochastic(B, z_{sem})$
 - for** each latent direction $k \in \{1, 2, \dots, n_{dirs}\}$ and $k \notin U$ **do**
 - Modify latent codes: $z_{pos} \leftarrow edit(z_{sem}, \alpha, k, +1)$ $z_{neg} \leftarrow edit(z_{sem}, \alpha, k, -1)$
 - Generate positive and negative images: $I_{pos} \leftarrow G.render(x_T, z_{pos})$ $I_{neg} \leftarrow G.render(x_T, z_{neg})$
 - Compute the average probability change for target class c : $\Delta_{pos} \leftarrow p_\theta(I_{pos} | c) - p_\theta(B | c)$ $\Delta_{neg} \leftarrow p_\theta(I_{neg} | c) - p_\theta(B | c)$
 - if** $\Delta_{pos} > max_effect$ **then**
 - $best_coordinate \leftarrow k$ $best_direction \leftarrow +1$ $max_effect \leftarrow \Delta_{pos}$
 - if** $\Delta_{neg} > max_effect$ **then**
 - $best_coordinate \leftarrow k$ $best_direction \leftarrow -1$ $max_effect \leftarrow \Delta_{neg}$
- Append $best_coordinate$ to C Append $best_direction$ to D Add $best_coordinate$ to U Update remaining images by removing sufficiently explained ones (low probability change) Decrease threshold: $\tau \leftarrow \min(\tau, max_effect)$

return Best coordinates C and directions D
